A MirrorSAR Case Study Based on the X-Band High Resolution Wide Swath Satellite (HRWS)

Josef Mittermayer, Gerhard Krieger, Allan Bojarski, Mariantonietta Zonno, Michelangelo Villano, and Alberto Moreira
Microwaves and Radar Institute, German Aerospace Center (DLR), Germany
josef.mittermayer@dlr.de

Abstract

The paper reports selected results of a concrete MirrorSAR mission analysis study with the planned X-band HRWS satellite as transmitter. The driving goal is a next generation global DEM with a much better performance compared to TanDEM-X. Three small passive receiver satellites are spanning differently sized interferometric baselines by flying interlaced helix orbits. Several system engineering topics associated to the MirrorSAR concept are discussed. The multistatic echo window timing is investigated including the allowed along-track separation between transmitter and receivers. The interaction between helix orbit baseline design, Doppler steering, and phase preserving MirrorSAR link geometry is analyzed. A DEM performance estimation concludes the paper.

1 Introduction

The paper comprises MirrorSAR relevant results of a DLR funded phase 0/A study carried out in collaboration with Airbus that is entitled High Resolution Wide Swath (HRWS) as well as results from further research work carried out at DLR. The Microwaves and Radar Institute of DLR has proposed the MirrorSAR mission concept to enhance the planned HRWS satellite [1] with a global digital elevation model (DEM) capability with unprecedented accuracy. The goal is to achieve a height error better than 2 m (90% point-to-point error) at a horizontal posting of 4 m x 4 m [2]. The available global DEM of TanDEM-X [3] provides a similar height performance but at a much wider posting of 12 m x 12 m.

1.1 The MirrorSAR Basic Concept

The main idea of MirrorSAR [2] is the distribution of the transmit (Tx) and receive (Rx) SAR functionality on different platforms, whereby the Rx satellites are reduced in functionality down to a space transponder. The Tx satellite additionally hosts the complex components of the radar signal receive chain. By means of a phase preserving MirrorSAR link (MirrorLink), the Rx satellites forward the ground reflected radar echoes back to the Tx satellite, as is illustrated in Figure 1.

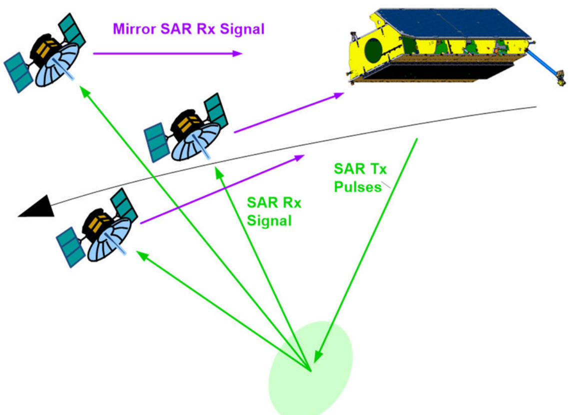

Figure 1: MirrorSAR acquisition geometry with HRWS as the master satellite.

On-board the Tx satellite, the down conversion for all received radar signals is carried out using the original transmit oscillator.

An indispensable part of MirrorSAR is the simultaneous acquisition of several Rx-baselines, which enable highly accurate and robust SAR interferometry. Large and small baselines are available simultaneously in one over-flight.

1.2 MirrorLink Options

In [4], two main options a MirrorLink were introduced. The first option is the use of a modulation that *preserves the phase* of the radar signal in the back channels from the Rx satellites to the Tx satellite. This can be achieved, for example, if the receiver satellites generate a high frequency signal (with an either microwave or optical carrier) that is amplitude modulated by the radar echo to be forwarded to the transmitter.

The availability of an optical link at the time when MirrorSAR enters into a critical design phase is considered very promising. However, in case that a phase preserving modulation is not available, [4] proposes the transmission of an additional reference signal from the Tx to the Rx satellites as is illustrated in Figure 2. This reference signal can be, for example, a copy of the imaging radar pulse transmitted to ground.

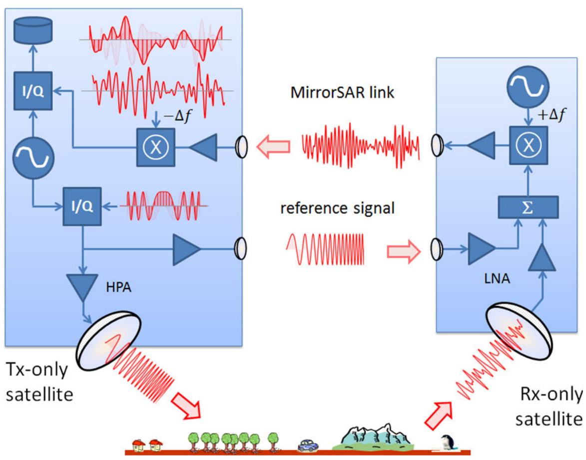

Figure 2: Double MirrorSAR synchronization.

https://ieeexplore.ieee.org/document/9472670

In this so-called double MirrorSAR synchronization, the reference signal is sent by using a low-gain link. The Rx satellite superimposes the reference signal to the radar echo. The overlaid signals are jointly frequency shifted by +Δf using a coherent mixer and radiated back to the Tx satellite, where the additional frequency shift is reversed before the signal is down-converted. The frequency shifts introduce phase errors, but are identical in the radar echo signal and the double mirrored reference signal.
In the echo window timing discussion below, the case of a double MirrorSAR synchronization with radar pulses as reference signal is analyzed.

2 HRWS MirrorSAR Geometry

2.1 Slant Range Geometry

The timing calculations as well as the DEM performance analysis are based on a TerraSAR-X orbit at 514 km altitude, and elevation beams of 20 km swath width each that overlap by 1 km. The incidence angles are given in Table 1. The total access range of beams 0 – 12 is above 240 km and allows for global coverage at an orbit altitude of 514 km. The higher angle beams 13 – 15 are less performant.

swath #	0	1	2	3	4	5	6	7	8	9	10	11	12	13	14	15
inci near [°]	30.0	31.7	33.4	35.1	36.7	38.2	39.7	41.1	42.5	43.8	45.1	46.4	47.6	48.7	49.8	50.9
inci far [°]	31.8	33.5	35.2	36.8	38.3	39.8	41.2	42.6	43.9	45.2	46.4	47.6	48.8	49.9	51.0	52.0

Table 1: Elevation beams for the DEM mode.

2.2 Helix Orbits and Rx-Baselines

A favorable orbit concept for the simultaneous echo acquisition by 3 Rx satellites is introduced by interlacing 3 helix orbits that fly all around a reference orbit that is defined by a virtual satellite Rx_0. For this analysis, Rx_0 flies a TerraSAR-X orbit. HRWS transmits the Tx radar pulses and trails Rx_0 on the reference orbit by 15 km.
Figure 3 shows the across-track and radial baselines between the Rx satellites in their maximum values with respect to the virtual Rx_0 position at their corresponding argument of latitude. The along-track baselines are not included in the figure. They are twice as long as the radial baselines. Baseline variations over the orbit result from the interlaced helical structure. In this paper, the underlying orbits are based on Kepler orbit simulations, similar as described [3]. Due to the Earth's rotation, the cross-track baselines in Earth fixed geometry show an inevitable deviation of 5-10% from the symmetric maximum values of Figure 3.

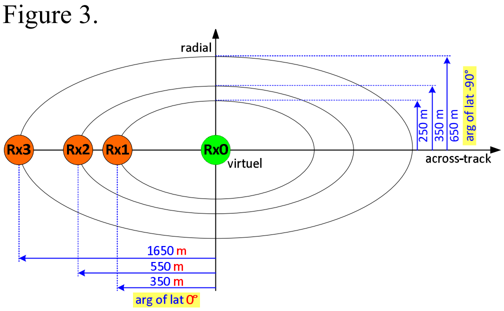

Figure 3: Rx baseline definition. Radial and across-track baselines are given in its maximum values. The Rx along-track baselines are twice the radial baselines.

Figure 4 provides in the left plot the virtual cross baselines Rx_0-Rx_i obtained from the orbit simulation versus argument of latitude. They always show the same sign and all the satellites Rx_1, Rx_2 and Rx_3 are always on the same side of the orbital plane that is defined by the reference orbit R_0. This is the result of an optimization of the MirrorLink beam width discussed in section 4. Figure 4 on the right provides the available minimum and maximum Rx baselines provided by Rx_1, Rx_2, and Rx_3.

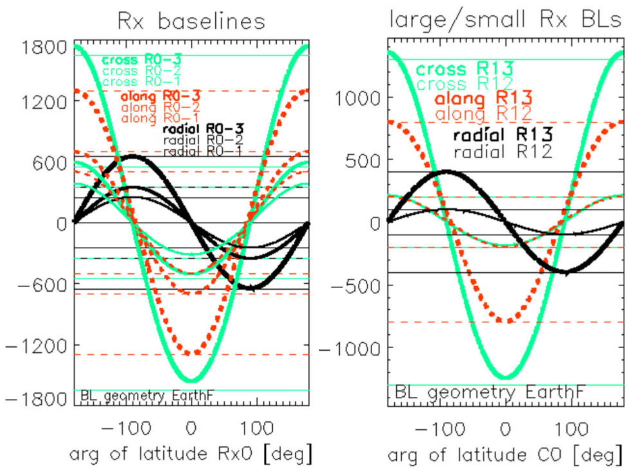

Figure 4: Rx-Baselines in Earth-fixed geometry in [m]. (left) With respect to the virtual satellite position Rx_0. The horizontal lines indicate the maximum inertial values in Figure 3. (right) Smallest and largest baselines resulting from Rx_1/Rx_2 and Rx_1/Rx_3, respectively.

3 Echo Window Timing

MirrorSAR carries out bi-static acquisitions with an additional analog forward of the received radar signals from the Rx satellites back to the Tx satellite.
Four important points need to be considered in addition to classical monostatic timing (diamond) diagram:

- The concept of the nadir echoes in pulsed radar needs to be re-defined for the bi-static acquisitions.
- The distances between the Tx and Rx satellites generate additional signal delays.
- The positions of the three different Rx satellite need to be considered.
- The recording capabilities of the Tx satellite: here, we assume a recording that is organized in pulse repetition intervals (PRIs). No echo window can trespass a PRI.

3.1 Nadir and Forward Reflection Area

In monostatic SAR, the nadir area contains the strongest ground reflections outside the desired acquisition area. The reflections originate from surfaces perpendicular to the incident signal direction. The nadir area is often defined by a so-called nadir angle θ_N that is rotational symmetric around the nadir direction. From experience with TerraSAR-X a reasonable θ_N for X-band is 1.5° [5].
For the bi-static acquisitions of MirrorSAR, we define a Forward Reflection Area (FRA) that describes the strongest reflections outside the desired swath. Figure 5 shows this area as bright ellipse below the Phase Center position PC in-between the Tx and Rx antenna positions that are separated by D_{RT} in along-track.

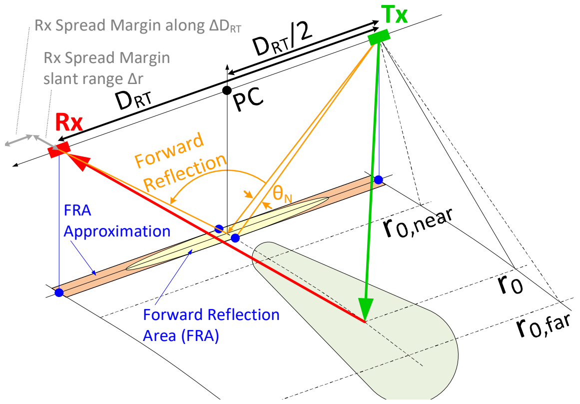

Figure 5: Bi-static acquisition geometry. The Tx satellite illuminates the desired swath and the Rx satellite receives. The strongest echoes outside the swath originate from forward reflections from the Tx to the Rx satellite.

For the sake of simplicity, the FRA is conservatively approximated to be "rectangular" and defined by the two satellites foot points and a symmetric right- and left-looking "nadir"-angle in cross-track direction. As Figure 5 shows, this provides four points on the ground (colored blue) that define the rectangle. The slant ranges r_0 in the imaged swath are defined from the virtual PC position in boresight geometry.

3.2 MirrorSAR Timing Diamond Diagram

The timing parameter design regulates the time relation between transmit pulses and FRA echoes with the receiving window. The following rules and assumptions were made in the calculation of the bi-static MirrorSAR diamond diagram:

- Spherical Earth model.
- Symmetric swath position as shown in Figure 5.
- Margin for range cell migration neglected, guard times before and after transmit events neglected, internal delays neglected.
- Simultaneous transmission of Tx pulses to ground and to Rx companions.
- Tx pulses can overlap in time with the echo receiving window (isolation by Tx and Rx satellites separation) as well as with the double mirrored synch pulses (isolation by different carriers in synch forward and radar+synch back channels).
- FRA: rectangular as in Figure 5 with 2.5° nadir angle.
- FRA echoes can overlap in time with Tx pulses in the synch fore channels (isolation by directivity) and the radar+synch back channels (isolation by diff. carriers).
- FRA echoes cannot overlap in time with receiving window, but can overlap with receiving window pulse extension (FRA echoes don't saturate receivers).
- Receiving window+extension can't exceed a single PRI from Tx pulse rising edge to next rising edge. The same restriction holds for double mirrored Tx synch pulses.

Several Rx companion satellites are modelled by a margin Δr that prolongs the receive path of the closest Rx companion by a margin of 1 km, and by a margin ΔD_{RT} of 2 km that prolongs the assumed distance from Tx satellite to the closest Rx satellite. These spread margins are illustrated in Figure 5 and cover the spread of the Rx companion satellites formation. The calculation of the FRA area is not modified by these margins (approximation). The margin Δr causes a prolongation of the focused receiving window in slant range. The margin ΔD_{RT} extends the runtime of the synch Tx pulses. Note that in an operational data take commanding, the actual companion positions need to be considered.

The rules and assumptions, the spread margins that introduce the Rx satellite formation as well as the slant range and elevation beam geometry defined in Table 1, were applied in the calculation of the bi-static diamond diagram. Figure 6 shows the result for an along-track separation of 13 km between HRWS and the closest companion. The Tx pulses transmitted to ground and to the Rx companion satellites are depicted in yellow. The blue Focused Echo Window (FEW) start and end times correspond to the near and far incidence angles of the related beam, respectively, and include the full signal path from Tx satellite to ground, and then on to the Rx satellite, and then from the Rx satellite back to the Tx satellite. The slant range margin Δr results in the solid extension on the right of the FEW. The required extension by the transmit pulse length in red completes the FEW to the longer echo window (EW). Due to the bi-static operation the Tx pulses can overlap with the EW. Limitations to the EW are the FRA echoes in gray that can't overlap with the FEW and by the single PRI interval limitation. The synch Tx pulses that are returned from the Rx satellites back to the Tx satellite within the MirrorSAR back channel are depicted in green color. The along-track spread margin ΔD_{RT} extends this window by the section in orange color. From the SAR performance calculations, a favorable target PRF of 6.2 kHz has been identified. This PRF is shown in the figure by the black horizontal line. Above this line, the swath number is identified. For the required full performance swaths 0 to 12 a PRF band from 5.8 to 6.45 kHz is required. The band is indicated by the dashed horizontal lines.

3.3 Along-Track Separation HRWS - Rx_i

In Figure 6, it can be observed that for PRF values above 7 kHz there are no more exchanged synch Tx pulses plotted (green + orange). The reason is the one PRI limitation.

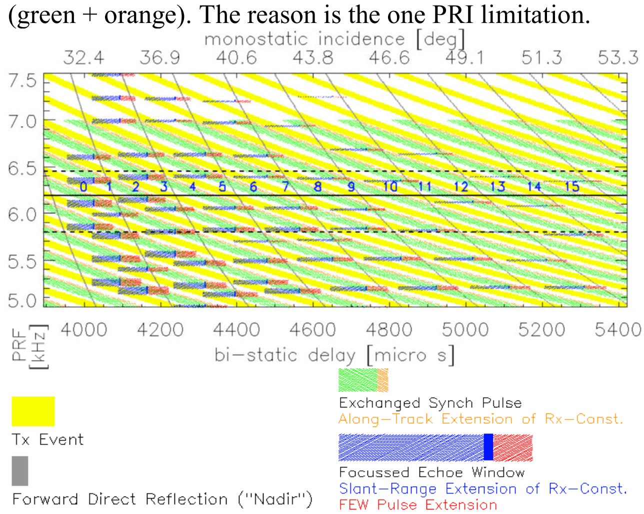

Figure 6: Diamond diagram for bi-static HRWS-MirrorSAR. Bottom axis is overall delay time. Top axis is equivalent to the monostatic incidence angle from the virtual PC.

The exchanged synch Tx pulses are not allowed to trespass the PRI borders as would be the case above 7 kHz for the along-track separation D_{RT} of 13 km. The possible along-track distances between HRWS and the closest Rx_i can be derived from Figure 7. For a certain PRF value, the minimum and maximum allowed separations D_{RT} are:

$$D_{RT,min}(n_{trav}) = \frac{n_{trav}}{PRF} \cdot \frac{c_0}{2}$$

$$D_{RT,max}(n_{trav}) = \left(\frac{n_{trav}+1}{PRF} - \frac{duty}{PRF}\right) \cdot \frac{c_0}{2} - \Delta D_{RT}$$

and are a function of the number of travelling pulses n_{trav} between HRWS and the companions. $D_{RT,min}$ is directly the rising edge of the Tx pulses, repeated after each PRI. $D_{RT,min}$ is calculated by subtracting the pulse length T_p and the along-track extension of the Rx constellation ΔD_R from an PRI.

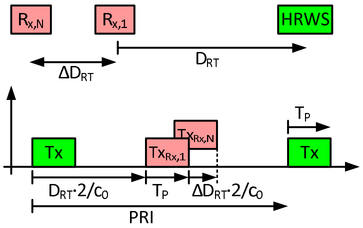

Figure 7: Along-track separations and one PRI limitation.

Figure 8 shows the valid combinations of D_{RT} (always for the companion closest to HRWS) and PRF values. The green areas show allowed combinations; the red ones are forbidden combinations. The large blue numbers indicate the number of travelling pulses in the double mirror link HRWS-companions-HRWS. The red numbers quantify the allowed separations, for example, 25.9 to 37.5 km for one travelling pulse.

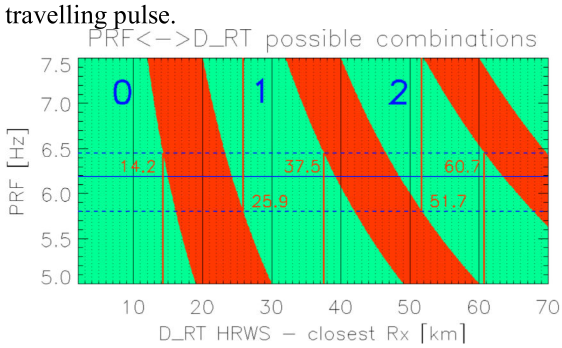

Figure 8: Allowed along-track separations between HRWS and the closest Rx satellite vs PRF.

4 MirrorLink and Doppler Steering

The MirrorLink is basically oriented parallel to the satellites flight direction, from the leading Rx satellites backward to the trailing Tx satellite. In the case of fixed mounted and non-steerable MirrorLink antennas, their beam widths need to cover:

- The maximum cross-track and radial baselines of the Rx_i satellites w.r.t. the Tx satellite on the Rx_0 reference orbit.
- The Doppler steering law. In approximation, the yaw and pitch steering of the Total Zero Doppler Steering (TZDS) [6] is assumed for Tx and Rx_i satellites.
- The bi-static acquisition geometry. As an approximation, additional yaw angles steer the Tx radar antenna towards forward direction and the Rx radar antennas towards backward. As is shown in Figure 9, the resulting total yaw angle is referred to as bi-static yaw.

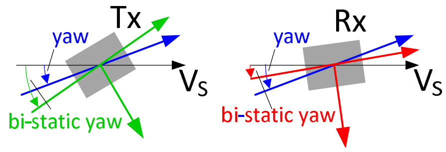

Figure 9: Yaw angle from Doppler steering in blue color. Bi-static yaw after additional forward/backward steering. Top-view into nadir direction.

The yaw angle from zero Doppler steering is very similar for the Tx and Rx satellites. It is important to note that due to the Doppler steering, the MirrorLink antennas do not point along the satellites velocity direction V_S but show a bias w.r.t. along-track and radial direction.

Figure 10 shows in the left plot in black color the bi-static yaw for two different look angles. The TZDS does not depend on look angle, but the additional yaw for bi-static forward / backward steering does. In red and green color are the off-velocity angles under which the TX satellite observes Rx_0 and Rx_3, respectively. For Rx_0, the angle is zero as Rx_0 flies the Tx orbit. Rx_3 shows the largest cross-track baseline. For better visibility, the sign of the bi-static yaw is inverted in the plot. The right plot shows the total combined off-velocity angle.

If the orbits are flown with the maximum cross-track baselines position shifted by 180° argument of latitude, the addition to the total combined off-velocity angle is less constructive and results in the required beam width of Figure 11. The demand on MirrorLink antenna beam width is reduced. Due to this, all the Rx_i should be always arranged on the identical side of the Tx satellite orbital plane (refer also to Figure 3). This allows for a minimized MirrorLink antenna beam width.

The derived required beam width of the MirrorLink antennas in the along/cross-plane results to 9°. In the same way, the required beam width in along/radial-plane can be estimated. However, the pitch angle in the TZDS is lower (monostatic values < 0.1°) and the counterbalancing effect is much smaller. Only from geometry, i.e., 15 km along-track distance and 2 x 650 m radial baseline, a required beam width of 5° results in the along/radial plane.

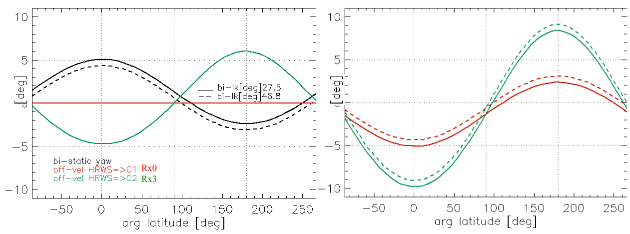

Figure 10: (left) Bi-static yaw (inverted sign) and off-velocity angle for observation of Rx_0 and Rx_3 from the Tx satellite. (right) Required beam width of MirrorLink antenna for unfavorable design of the cross-track baselines.

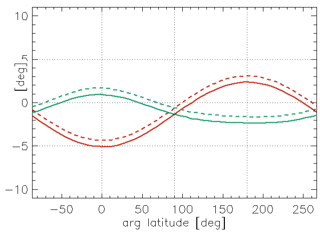

Figure 11: Required beam width of MirrorLink antenna for favorable design of cross-track baselines.

5 DEM Mode & Performance

5.1 SAR Performance

The SAR performance was calculated based on the key parameters in Table 2. For elevation beams 0 to 12, a summary of the estimated SAR performance parameters is provided in the bottom part of the table.

Tx SAR antenna	6 m x 1.4 m (azimuth x elevation)
Rx SAR antennas	3 m x 1 m
Tx average power	2.3 kW
Tx bandwidth	200 MHz
NF + losses + margin	7.4 dB
SAR image resolution	1.5 m azimuth x 1.5 m ground range
Allowed Rx pointing error	0.05°
AASR / RASR	< -19.7 dB / < -19 dB
NESZ	> -19 dB
Number range looks	1.2 (beam 0) to 1.7 (beam 12)
Number azimuth looks	1.0

Table 2: HRWS-MirrorSAR system key parameters (top) and SAR performance parameters summary (bottom)

An intensive analysis of the effect of pointing errors has been performed. The Tx pointing was assumed to be w/o error in comparison to the less stabilized smaller Rx satellites. It was concluded that a pointing error of 0.05° for the Rx satellites is still acceptable. This conclusion is driven by the Azimuth Ambiguity to Signal Ratio (AASR). In the next mission phase, performance and mission design improvements by advanced AASR suppression techniques need to be considered, e.g. staggered SAR [7],[8].

5.2 DEM Performance

The DEM performance has been derived from the SAR system and performance parameters in Table 2, the interferometric parameters in Table 3, and the geometry resulting from the Rx baselines provided in Figure 4 that is based on a TerraSAR-X like reference orbit.

Sigma$_0$ - Model	Ulaby soil&rock, 90th percentile
IRF sidelobe suppression	no
ground posting	4 m x 4 m (azimuth x gr, range)
interf. looks (no overlap)	4/1.5 x 4/(1.2 to 1.7) =8.9 to 6.3
correlation coefficients:	
temporal	1.0
quantization (4bit)	0.989*
range spectral shift	0.984* (Baseline decorrelation)
misregis. Az. and Doppler shift	0.989*
volume	0.985

Table 3: HRWS-MirrorSAR DEM performance input parameters. (*values are taken from [1]).

The acquisition geometry defines the Height of Ambiguities (HoA) provided in Figure 12. On top, the HoA for ascending and descending orbits is shown in its variation of the look angle range of beams 0 to 12. The bottom plot selects from ascending and descending orbit the minimum HoA available at each target latitude. The HoA and the SAR performance provide the DEM performance in the upper plot of Figure 13. It is expressed in 90% point to point height error (refer to [1]).

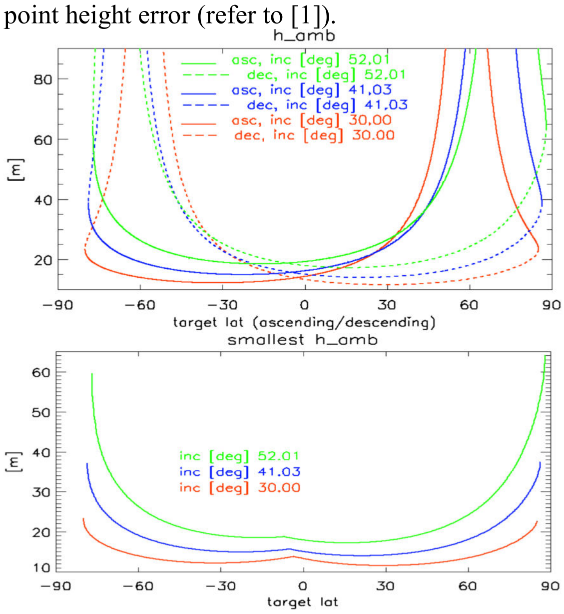

Figure 12: HoA resulting for smallest Rx baseline. (top) HoA for minimum, center, and maximum look angle in ascending as well as descending orbits. (bottom) Selection of only the minimum HoA out of ascending/descending.

The horizontal posting is 4 x 4 m, and the required minimum height error of 2 m is obtained for almost all latitudes in the interval [-60°,60°]. The beams 0-12 cover 240 km ground range at the equator, that are required for global coverage (refer to section 2.1). The upper incidence angle of beam 12 is indicated by the horizontal dashed line. Only few combinations of higher incidence angles and latitudes show a height error up to 3 m.

The DEM performance for 0.05° Rx pointing error is shown in Figure 13. The DEM performance was calculated by treating the azimuth ambiguities as incoherent noise only. In the next mission phase, the influence of coherent ambiguities on the DEM performance needs to be included. This topic is still under research, e.g. [9],[10],[11]. In Figure 13, an undulating DEM performance variation vs. incidence angle is obvious, caused by the sequence of different elevation beams. A simple mutual shift of the elevation beam maxima between the acquisitions with different basslines, as is done e.g., in TanDEM-X, is not possible due to the single pass acquisition of the baselines. Current research connects the multi-static zero Doppler steering with the antenna pattern overlap in a single pass multi-baseline scenario [12]. Although azimuth overlaps are evaluated, it provides valuable inputs to the elevation beam design for multiple baselines.

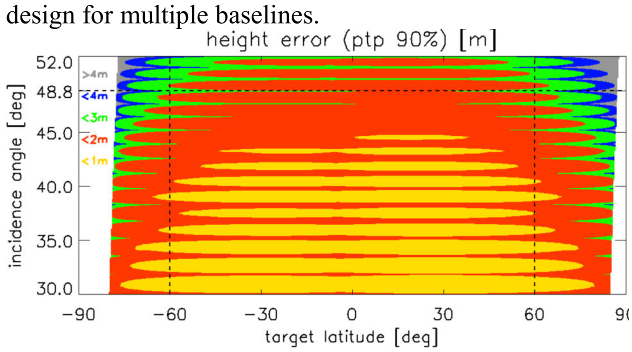

Figure 13: Height error derived from largest available Rx baselines for a pointing error of 0.05°.

6 Discussion

The paper described a concrete design for a MirrorSAR DEM system based on the HRWS sensor as radar illuminator. The SAR performance was estimated and it confirmed the underlying system concept and acquisition mode design. The estimated DEM performance provided the intended one. A height error better than 2 m was achieved at a horizontal posting of 4 m in both ground dimensions. The 2 m height error is obtained within 60° of southern and northern latitudes. For latitudes lower 45° the height error is often even below 1 m. It should be kept in mind that only one orbital configuration has been analyzed. In the mission operation, the baselines can be changed to also provide excellent height errors at higher latitudes.

The DEM performance is an improvement of several times compared to the TanDEM-X mission. A similar height error is obtained with a horizontal posting that is reduced by a factor of 9.

The paper discussed several system engineering topics that are relevant for a phase B mission design. An elaborated helix-orbit concept has been established that provides the required small and large Rx-baselines at one overflight.

The echo window timing was extended to simultaneous bi-static acquisition with several Rx satellites. The along-track separation between the HRWS satellite working as transmitter and the Rx satellites was connected to the acquisition timing parameters, and the standard echo window limitation to one PRI of pulsed radars was converted into possible along-track separations between HRWS transmitter and the receiving satellites. A reasonable separation should be between 26 and 37.5 km.

The interaction between Doppler-Steering-Law, bi-static acquisition geometry, and the Rx-baseline configuration was analyzed along the orbit. It was found that all the Rx satellites should be on the same side of the reference orbit plane. From this analysis, requirements were derived for the required MirrorLink antenna beam width. The beam width should be 9° in cross-track and 5° in radial dimensions.

The effect of pointing errors on the SAR and DEM performance was analyzed under the premise of a technically advanced and highly accurate HRWS satellite in transmit, and less accurate but highly cost-effective Rx satellites. A pointing requirement of better than 0.05° was derived for the Rx satellites.

The DEM performance illustrates the great leap in quality of MirrorSAR as a continuation of the already very good and well-established TanDEM-X mission.

There is a need for further optimization of DEM and mission performance. Examples include the impact of coherent ambiguities on the DEM performance, the design of elevation beams for the various acquisition baselines, and the potential alleviations in the mission design due to advanced techniques for azimuth ambiguity suppression.

7 Literature

[1] J. Janoth, M. Jochum, L. Petrat, T. Knigge, “High Resolution Wide Swath – The next generation X-Band Mission”, Proc. of IGARSS 2019.

[2] M. Zonno, G. Krieger, , M. Rodriguez-Cassola ,J. Mittermayer, and A. Moreira, “A MirrorSAR-based single-pass dual-baseline SAR interferometer for the generation of very high quality DEMs”, Proc. of EUSAR 2018, Aachen, 2018.

[3] G. Krieger, A. Moreira, H. Fiedler, I. Hajnsek, M. Werner, M. Younis, and M. Zink, “TanDEM-X: A Satellite Formation for High-Resolution SAR Interferometry”, IEEE Transactions on Geoscience and Remote Sensing, vol. 45, no. 11, pp. 3317–3341, 2007.

[4] G. Krieger, M. Zonno, J. Mittermayer, A. Moreira, S. Huber, M. Rodriguez-Cassola, “MirrorSAR: A Fractionated Space Transponder Concept for the Implementation of Low-Cost Multistatic SAR Missions”, Proc. of EUSAR 2018, Aachen, 2018.

[5] S. Wollstadt and J. Mittermayer, “Nadir Margins in TerraSAR-X Timing Commanding”, Proc. of CEOS SAR Calibration and Validation Workshop, 2008.

[6] H. Fiedler, E. Boerner, J. Mittermayer, and G. Krieger, “Total zero Doppler steering—A new method for minimizing the Doppler centroid,” IEEE Geosci. Remote Sens. Lett., vol. 2, no. 2, pp. 141–145, Apr. 2005.

[7] N. Ustalli, M. Villano, “Impact of Ambiguity Statistics on Information Retrieval for Conventional and Novel SAR Modes,” Proceedings of the IEEE 2020 Radar Conference, Florence, Italy, 21-25 September 2020.

[8] M. Villano, G. Krieger, M. Jäger, A. Moreira, “Staggered SAR: Performance Analysis and Experiments with Real Data,” IEEE Transactions on Geoscience and Remote Sensing, vol. 55, no. 11, pp. 6617-6638, Nov. 2017.

[9] M. Villano, G. Krieger, “Impact of Azimuth Ambiguities on Interferometric Performance,” IEEE Geoscience and Remote Sensing Letters, vol. 9, no. 5, pp.896-900, Sept. 2012.

[10] M. Villano, G. Krieger, “Accounting for Azimuth Ambiguities in Interferometric Performance Analysis,” IEEE International Geoscience and Remote Sensing Symposium (IGARSS) 2012, Munich, Germany, 22-27 July 2012.

[11] N. Ustalli, M. Villano, “Impact of Ambiguity Statistics on Information Retrieval for Conventional and Novel SAR Modes,” Proceedings of the IEEE 2020 Radar Conference, Florence, Italy, 21-25 September 2020.

[12] J. Mittermayer, G. Krieger, S. Wollstadt, “Numerical Calculation of Doppler Steering Laws in Bi- and Multistatic SAR”, submitted to TGRS, minor revision in progress.